Biomedical Optics EXPRESS

In vivo visualization of skin inflammation by optical coherence tomography and two-photon microscopy

Bumju Kim,[1] Seung Hun Lee,[1] Calvin J. Yoon,[2] Yong Song Gho,[3,4] G-One Ahn,[2,3] and Ki Hean Kim[1,2,*]

[1]*Department of Mechanical Engineering, Pohang University of Science and Technology, 77 Cheongam-ro, Nam-gu, Pohang, Gyeongbuk 790-784, South Korea*
[2]*Division of Integrative Biosciences and Biotechnology, Pohang University of Science and Technology, 77 Cheongam-ro, Nam-gu, Pohang, Gyeongbuk 790-784, South Korea*
[3]*Department of Life Science, Pohang University of Science and Technology, 77 Cheongam-ro, Nam-gu, Pohang, Gyeongbuk 790-784, South Korea*
[4] *Division of Molecular and Life Sciences, Pohang University of Science and Technology, 77 Cheongam-ro, Nam-gu, Pohang, Gyeongbuk 790-784, South Korea*
[*]*kiheankim@postech.edu*

Abstract: Inflammation is a non-specific immune response to injury intended to protect biological tissue from harmful stimuli such as pathogens, irritants, and damaged cells. *In vivo* optical tissue imaging has been used to provide spatial and dynamic characteristics of inflammation within the tissue. In this paper, we report *in vivo* visualization of inflammation in the skin at both cellular and physiological levels by using a combination of label-free two-photon microscopy (TPM) and optical coherence tomography (OCT). Skin inflammation was induced by topically applying lipopolysaccharide (LPS) on the mouse ear. Temporal OCT imaging visualized tissue swelling, vasodilation, and increased capillary density 30 min and 1 hour after application. TPM imaging showed immune cell migration within the inflamed skin. Combined OCT and TPM was applied to obtain complementary information from each modality in the same region of interest. The information provided by each modality were consistent with previous reports about the characteristics of inflammation. Therefore, the combination of OCT and TPM holds potential for studying inflammation of the skin.

OCIS codes: (180.2520) Fluorescence microscopy; (180.4315) Nonlinear microscopy; (110.4500) Optical coherence tomography; (170.3880) Medical and biological imaging; (170.6920) Time-resolved imaging.

References and links

1. S. C. Gad, "The mouse ear swelling test (MEST) in the 1990s," Toxicology **93**(1), 33–46 (1994).
2. D. A. Basketter and E. W. Scholes, "Comparison of the local lymph node assay with the guinea-pig maximization test for the detection of a range of contact allergens," Food Chem. Toxicol. **30**(1), 65–69 (1992).
3. V. Kalchenko, Y. Kuznetsov, D. Preise, I. Meglinski, and A. Harmelin, "Ear swelling test by using laser speckle imaging with a long exposure time," J. Biomed. Opt. **19**(6), 060502 (2014).
4. K. G. Phillips, Y. Wang, D. Levitz, N. Choudhury, E. Swanzey, J. Lagowski, M. Kulesz-Martin, and S. L. Jacques, "Dermal reflectivity determined by optical coherence tomography is an indicator of epidermal hyperplasia and dermal edema within inflamed skin," J. Biomed. Opt. **16**(4), 040503 (2011).
5. V. Kalchenko, Y. Kuznetsov, I. Meglinski, and A. Harmelin, "Label free in vivo laser speckle imaging of blood and lymph vessels," J. Biomed. Opt. **17**(5), 050502 (2012).
6. V. V. Kalchenko, Y. L. Kuznetsov, and I. V. Meglinski, "Visualisation of blood and lymphatic vessels with increasing exposure time of the detector," Quantum Electron. **43**(7), 679–682 (2013).
7. D. Huang, E. A. Swanson, C. P. Lin, J. S. Schuman, W. G. Stinson, W. Chang, M. R. Hee, T. Flotte, K. Gregory, C. A. Puliafito, and et, "Optical coherence tomography," Science **254**(5035), 1178–1181 (1991).

#235702 Received 11 Mar 2015; revised 1 Jun 2015; accepted 9 Jun 2015; published 15 Jun 2015

8. Y. Jung, S. Dziennis, Z. Zhi, R. Reif, Y. Zheng, and R. K. Wang, "Tracking dynamic microvascular changes during healing after complete biopsy punch on the mouse pinna using optical microangiography," PLoS ONE **8**(2), e57976 (2013).
9. B. J. Vakoc, R. M. Lanning, J. A. Tyrrell, T. P. Padera, L. A. Bartlett, T. Stylianopoulos, L. L. Munn, G. J. Tearney, D. Fukumura, R. K. Jain, and B. E. Bouma, "Three-dimensional microscopy of the tumor microenvironment in vivo using optical frequency domain imaging," Nat. Med. **15**(10), 1219–1223 (2009).
10. C. Blatter, J. Weingast, A. Alex, B. Grajciar, W. Wieser, W. Drexler, R. Huber, and R. A. Leitgeb, "In situ structural and microangiographic assessment of human skin lesions with high-speed OCT," Biomed. Opt. Express **3**(10), 2636–2646 (2012).
11. S. Yousefi, J. Qin, Z. Zhi, and R. K. Wang, "Label-free optical lymphangiography: development of an automatic segmentation method applied to optical coherence tomography to visualize lymphatic vessels using Hessian filters," J. Biomed. Opt. **18**(8), 086004 (2013).
12. T. Takano, C. B. Clish, K. Gronert, N. Petasis, and C. N. Serhan, "Neutrophil-mediated changes in vascular permeability are inhibited by topical application of aspirin-triggered 15-epi-lipoxin A4 and novel lipoxin B4 stable analogues," J. Clin. Invest. **101**(4), 819–826 (1998).
13. E. L. Campbell, N. A. Louis, S. E. Tomassetti, G. O. Canny, M. Arita, C. N. Serhan, and S. P. Colgan, "Resolvin E1 promotes mucosal surface clearance of neutrophils: a new paradigm for inflammatory resolution," FASEB J. **21**(12), 3162–3170 (2007).
14. K. Gronert, S. P. Colgan, and C. N. Serhan, "Characterization of human neutrophil and endothelial cell ligand-operated extracellular acidification rate by microphysiometry: impact of reoxygenation," J. Pharmacol. Exp. Ther. **285**(1), 252–261 (1998).
15. S. P. Colgan, C. N. Serhan, C. A. Parkos, C. Delp-Archer, and J. L. Madara, "Lipoxin A4 modulates transmigration of human neutrophils across intestinal epithelial monolayers," J. Clin. Invest. **92**(1), 75–82 (1993).
16. A. D. Luster, R. Alon, and U. H. von Andrian, "Immune cell migration in inflammation: present and future therapeutic targets," Nat. Immunol. **6**(12), 1182–1190 (2005).
17. C. Godson, S. Mitchell, K. Harvey, N. A. Petasis, N. Hogg, and H. R. Brady, "Cutting edge: lipoxins rapidly stimulate nonphlogistic phagocytosis of apoptotic neutrophils by monocyte-derived macrophages," J. Immunol. **164**(4), 1663–1667 (2000).
18. B. H. Zinselmeyer, J. N. Lynch, X. Zhang, T. Aoshi, and M. J. Miller, "Video-rate two-photon imaging of mouse footpad - a promising model for studying leukocyte recruitment dynamics during inflammation," Inflamm. Res. **57**(3), 93–96 (2008).
19. D. Kreisel, R. G. Nava, W. Li, B. H. Zinselmeyer, B. Wang, J. Lai, R. Pless, A. E. Gelman, A. S. Krupnick, and M. J. Miller, "In vivo two-photon imaging reveals monocyte-dependent neutrophil extravasation during pulmonary inflammation," Proc. Natl. Acad. Sci. U.S.A. **107**(42), 18073–18078 (2010).
20. A. Klinger, R. Orzekowsky-Schroeder, D. von Smolinski, M. Blessenohl, A. Schueth, N. Koop, G. Huettmann, and A. Gebert, "Complex morphology and functional dynamics of vital murine intestinal mucosa revealed by autofluorescence 2-photon microscopy," Histochem. Cell Biol. **137**(3), 269–278 (2012).
21. C. Li, R. K. Pastila, C. Pitsillides, J. M. Runnels, M. Puoris'haag, D. Côté, and C. P. Lin, "Imaging leukocyte trafficking in vivo with two-photon-excited endogenous tryptophan fluorescence," Opt. Express **18**(2), 988–999 (2010).
22. Y. Zeng, B. Yan, Q. Sun, S. K. Teh, W. Zhang, Z. Wen, and J. Y. Qu, "Label-free in vivo imaging of human leukocytes using two-photon excited endogenous fluorescence," J. Biomed. Opt. **18**(4), 040504 (2013).
23. L. E. Grosberg, A. J. Radosevich, S. Asfaha, T. C. Wang, and E. M. Hillman, "Spectral characterization and unmixing of intrinsic contrast in intact normal and diseased gastric tissues using hyperspectral two-photon microscopy," PLoS ONE **6**(5), e19925 (2011).
24. S. H. Diks, S. J. van Deventer, and M. P. Peppelenbosch, "Lipopolysaccharide recognition, internalisation, signalling and other cellular effects," J. Endotoxin Res. **7**(5), 335–348 (2001).
25. P. Xiao, Q. Li, Y. Joo, J. Nam, S. Hwang, J. Song, S. Kim, C. Joo, and K. H. Kim, "Detection of pH-induced aggregation of "smart" gold nanoparticles with photothermal optical coherence tomography," Opt. Lett. **38**(21), 4429–4432 (2013).
26. B. Jeong, B. Lee, M. S. Jang, H. Nam, S. J. Yoon, T. Wang, J. Doh, B. G. Yang, M. H. Jang, and K. H. Kim, "Combined two-photon microscopy and optical coherence tomography using individually optimized sources," Opt. Express **19**(14), 13089–13096 (2011).
27. B. Kim, T. J. Wang, Q. Li, J. Nam, S. Hwang, E. Chung, S. Kim, and K. H. Kim, "Combined two-photon microscopy and angiographic optical coherence tomography," J. Biomed. Opt. **18**(8), 080502 (2013).
28. A. S. Nam, I. Chico-Calero, and B. J. Vakoc, "Complex differential variance algorithm for optical coherence tomography angiography," Biomed. Opt. Express **5**(11), 3822–3832 (2014).
29. M. T. Tsai, F. Y. Chang, C. K. Lee, C. S. Gong, Y. X. Lin, J. D. Lee, C. H. Yang, and H. L. Liu, "Investigation of temporal vascular effects induced by focused ultrasound treatment with speckle-variance optical coherence tomography," Biomed. Opt. Express **5**(7), 2009–2022 (2014).
30. D. J. Ravnic, M. Konerding, J. P. Pratt, T. Wolloscheck, H. T. Huss, and S. J. Mentzer, "Inflammation-responsive focal constrictors in the mouse ear microcirculation," J. Anat. **209**(6), 807–816 (2006).

#235702 Received 11 Mar 2015; revised 1 Jun 2015; accepted 9 Jun 2015; published 15 Jun 2015

1. Introduction

Inflammation is a non-specific immune response to injury intended to protect biological tissue from harmful stimuli such as pathogens, irritants, and damaged cells, and is also intended to promote tissue repair. Inflammation can range from a variety of degrees of severity for which therapy are being developed.

There are two main methods for studying inflammation: observation of morphological and physiological change and conducting cellular and molecular analyses. The former may include symptoms of redness, swelling, heat, and vasodilation, which were observed by mouse ear swelling test (MEST) [1] or rat allergy tests in previous studies [2]. However, these tests are highly subjective, which led to the usage of optical analysis through LSI and OCT technology to quantitatively study the inflammatory response [3, 4]. Laser speckle imaging (LSI) is a quick, label free imaging technique that has been used to observe changes in vasculature. Speckle changes between static and flowing objects are detected, allowing this technique to capture the very slow blood flow of microvasculature and lymph flow of lymph vessels given long exposure time [3, 5, 6]. However, characterization of inflammation by LSI is limited to angiography due to its 2D imaging nature, unable to provide structural or thickness information. 3D information can be provided by optical coherence tomography (OCT) [7], which has been used extensively to observe tissue microstructures and vasculature [8–10]. OCT uses the back-reflection of light from tissue and can observe tissue microstructure and vasculature at less than 10 micron resolution. Structural OCT has found that epidermal hyperplasia and dermal edema can be measured by dermal reflectivity [4]. Moreover, with high-resolution OCT, lymphatic vessels can be detected as vascular structures with much less scattering [11]. Angiographic OCT, which is an advanced OCT technique, has been used to visualize redistribution of vasculature vessel size during wound healing after inducing injury on the moue ear [8].

Conversely, with regards to cellular and molecular analyses of inflammation, conventional methods such as H&E staining, myeloperoxidase absorbance spectrophotometry [12], PMN transmigration assay, immunofluorescence, flow cytometry, and microphysiometry, have significantly contributed to our understanding of inflammation [13–17]. However, the extensive sacrifices, and inherently, deviations from physiological conditions limit knowledge about the *in vivo* dynamics of immune pathogenesis. Therefore, in order to observe cell dynamics, fluorescence microscopic techniques such as two-photon microscopy (TPM) has been used. TPM is one of the most widely used fluorescence microscopic imaging techniques that provide sub-micron resolution, 3D fluorescence images with high imaging depth and minimal photo damage, and has been used to observe the dynamics of immune cells labeled with fluorescent proteins or other exogenous labels in several regions of the mouse such as lung, heart, lymph node, footpad, and intestine [18–20]. However, preparation of labeled samples is time consuming as target-specific conditions for research must be met. In addition, labeling is not yet suitable for human immune cell studies. Thus recently, immune cell response has successfully been imaged label-free *in vitro* and *in vivo* by autofluorescence in various tissues [21–23]. Through tryptophan autofluorescence, immune cells of mouse ear were imaged *in vivo* [21], however, with compromised imaging depth due to the short excitation wavelength. Through NADH, human immune cells were imaged *in vitro* [22]. In addition, autofluorescence imaging has been conducted to visualize cells during the wound healing process of the small intestinal mucosa [23]. Evidently, autofluorescence imaging has emerged as a method of visualizing immune cells in several tissues, but to our knowledge, has not yet been conducted on the skin.

In this paper, we use OCT to observe physiological changes and TPM to observe cellular level changes of lipopolysaccharide (LPS)-induced inflammation in the mouse ear. Utilizing the complementary information provided by each system, we image the various symptoms of inflammation over time. Through structural OCT, we investigate the changes in tissue

#235702 Received 11 Mar 2015; revised 1 Jun 2015; accepted 9 Jun 2015; published 15 Jun 2015

structure and size. Through angiographic OCT, we observe vascular changes. In addition, through autofluorescence imaging by TPM, we show cellular dynamics. Following, we image the inflammation model with the combined OCT and TPM system, which allows us to image the same tissue location while eliminating any artifacts that may have been caused from transporting the sample between the two imaging systems.

2. Materials and methods

2.1 Mouse model preparation

A Balb/c mouse, 8 weeks old, was used as the animal model for hosting the immune response. The mouse was anesthetized with isoflurane gas and the body temperature was maintained with an electronic heating pad. The head of the mouse was held with custom-made ear bars to stabilize head movement from breathing motions and the ears were attached flatly onto slide glass by using double sided tape. To induce the inflammation response, we selected LPS, a component of gram negative bacterial membrane, which is widely used in inflammatory studies [24]. The mouse ears were pricked several times by using an insulin syringe needle (26 gauge) and spread with 20 μl (125 μg/ml) LPS. Balb/c mouse model was obtained from the Jackson Laboratory, and bred at the animal facility of POSTECH Biotech Center (PBC) under specific pathogen-free conditions.

2.2 Imaging system

Optical configurations of OCT and TPM system were based on a previous imaging setup [25, 26]. The conventional OCT system was equipped with a 50 kHz swept source laser (SSOCT-1310, Axsun), with a center wavelength of 1310 nm, bandwidth of 107 nm, and an output power of 26 mW. Light from the laser source was split to 90:10 ratio. 90% of the light was sent to the interferometry system and 10% of the light went for fiber Bragg grating (FBG) and detection by photo detector (PDB110C) to generate a trigger signal. In the interferometer, the light was split again to a 90:10 ratio by fiber coupler (FC) as sample arm and reference arm. The illumination beam of the sample arm was sent to the galvanometric x-y scanner (GS1, GVS002, Thorlabs) and was focused at the sample by a 5X scan lens (SL, LSM03, Thorlabs). The remaining 10% beam was sent to the reference arm for path length delay. Both beams, which back-reflect from the sample and reference arms, were recombined in the detection arm and detected by a balanced photo detector (PD, HCA-S-200M, FEMTO). Finally, OCT data was digitized by a data acquisition board (ATS9350, AlazarTech). This OCT system provides 20 μm lateral resolution and 7.1 μm axial resolution images.

The TPM system used a wavelength tunable Ti-sapphire laser for the light source (Chameleon II, Coherent) which was 140 fs pulse width and 80 MHz pulse repetition. Laser power was controlled by a combination of the polarization beam splitter (PBS) and half wave plate (HWP). Attenuated excitation beam was sent to the x-y galvanometric scanner (GS2, 6215H, Cambridge Technology). Following, the diameter of the excitation beam was magnified 5 times by a combination of scan (SCL) and tube lenses (TL), and was sent to a remodeled microscope (BX51, Olympus). In the microscope, the laser was diverted by the upper dichroic mirror (DM1, 680DCSP, Chroma) and was sent to transmit through the lower one (DM2, 680DCLP, Chroma). Finally, excitation beam passing through a water immersion objective lens (OL, XLUMPlanFLN, Olympus 20X, 1.0 NA), which was mounted on a piezo electric controller (PEC, P-725.4CLm PI) for z-scanning, was focused onto the sample for two photon emission. Back emission light from the sample was collected by the objective lens and reflected by one dichroic mirror (DM2) to another dichroic mirror (DM3, 430DCLP, Chroma), which split the emission light into autofluorescence and second harmonic generation (SHG) signals. Each signal was collimated by convex lens and detected by photo multiplier tubes (PMT, H7421-40, Hamamatsu). Signal from the PMT was converted to intensity data by a custom-made photon counter and acquired by a Labview board (PCI-6602,

#235702 Received 11 Mar 2015; revised 1 Jun 2015; accepted 9 Jun 2015; published 15 Jun 2015

Labview), mounted into the computer, and was displayed in real-time after processing. Excitation laser wavelength selected at 780 nm (45mW at sample) was used for auto-fluorescence imaging.

The combined system is an integration of the two aforementioned systems with individually optimized light sources. In particular, there was no significant difference in the overall TPM system configuration. The dichroic mirror at the sample arm overlaps the beam paths of OCT and TPM. This system is described in detail in a previous report [27]. OCT in the combined system provides 10 μm lateral resolution and 7.1 μm axial resolution images though using a different numerical aperture (NA).

2.3 Data acquisition and processing

OCT was imaged with 4.5 by 4.5 mm FOV at 1000 by 1000 pixels. Each cross sectional scan was repeated 8 times for angiographic imaging. The imaging time for one cross section is 0.02 sec and 160 sec for full volume acquisition. The OCT data was processed by MATLAB. A complex differential variance algorithm [28] was used for angiographic OCT images in order to reduce bulk motion of the mouse ear. The differential variance of the complex data in the 8 repetition images was calculated for each y-position. Sample movement in the z-axis was averaged and used to cancel motion artifact. The thickness of the mouse ear was measured by using threshold-based surface finding in the structural OCT images. For each depth scan, a percentage threshold was selected within the range of minimum and maximum intensity values to represent the surface of the mouse ear. To avoid strong signal from hair, height coordinates of adjacent surface pixels were compared to ensure that the difference of these coordinates were within 5 pixels, where surpassing would be considered discontinuous and the height would then be assumed the same as that of the adjacent lower surface.

TPM was imaged with 300 by 300 micrometer FOV at 512 by 512 pixels. In order to create a 3D volumetric image, a piezo translator guided the objective lens along the z-axis by 2 micrometer increments. 2 PMTs were used for 2-channel imaging (PMT1: less than 430 nm, SHG depicted in red, PMT2: 430-680 nm, depicted in green). The TPM imaging time was 7.8 seconds per frame with 30 μsec exposure per pixel. The time-lapse TPM images were processed to distinguish mobile cells. These TPM images had high background signal because of autofluorescence imaging. The standard deviations of 4 consecutive time-lapse images were calculated. Pixel coordinates with lower standard deviation were those of stationary background, while coordinates with higher standard deviation were those of moving signal. Stationary background signal was reduced to present moving signal, which included signal from blood vessels and mobile immune cells.

The combined OCT and TPM system had a smaller OCT FOV (1 by 1 mm) and thus the pixel size was reduced to 500 by 500 pixels. The FOVs of OCT and TPM were overlapped by comparing the images of a phantom that was created by embedding 2μm yellow green microspheres and hair strand in 2% agarose gel.

3. Results

3.1 OCT results

The mouse ear was imaged before, 30 min and 1 h after LPS treatment with conventional OCT to observe the physiological changes of tissue during the inflammation response, as shown in Fig. 1(a)-1(f). Structural and angiography OCT images taken before LPS treatment, Fig. 1(a) and 1(d) respectively, clearly show the mouse ear structures such as the epidermis, dermis, and cartilage, and blood vessel distribution. The structural OCT images 30 min after LPS treatment, Fig. 1(b), showed that the thickness of the mouse ear can be observed to increase over time. In addition, the flattening of the winding epidermal surface due to tissue swelling was also observed. Moreover, the overall intensity signal of the tissue was observed to decrease after treatment. The angiographic OCT images 30 min after treatment showed a

#235702 Received 11 Mar 2015; revised 1 Jun 2015; accepted 9 Jun 2015; published 15 Jun 2015

significant increase in signal from peripheral vasculature surrounding the main blood vessels, as can be seen in Fig. 1(e).

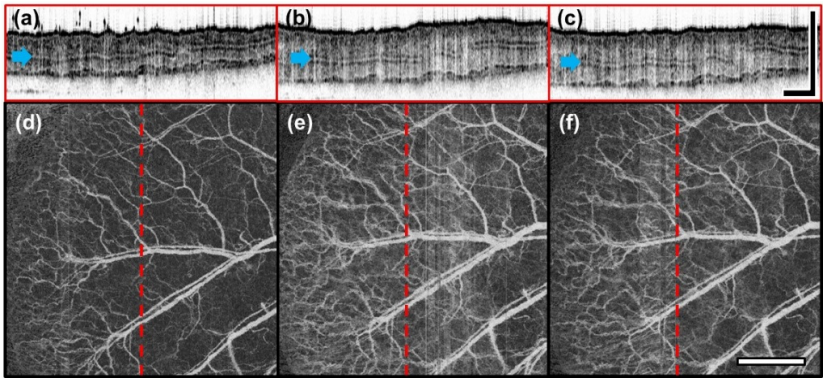

Fig. 1. Structural and angiographic OCT images before and after induction of inflammation taken at 30 min intervals (a, d: untreated, b, e: 30 min, c, f: 1 h) show progression of tissue swelling and vasodilation. Structural OCT images are presented as cross sectional views (a-c). The position of these images are indicated by red dashed lines on the angiographic OCT images (d-f). The blue arrows point to the cartilage. (Scale bar: 1 mm).

From the results obtained by structural and angiographic OCT images of 30 min (Fig. 1(b), 1(e)) and 1 h (Fig. 1(c), 1(f)) after treatment, we can observe that tissue swelling and vasodilation can sustain for over an hour. Quantitatively, the average thickness of LPS treated mouse ear compared to that of the untreated (247.63 μm ± 18.84 μm) shows a 27.56% increase at 30 min (315.03 μm ± 24.58 μm), followed by an insignificant 1.86% decrease at 1 h (311.28 μm ± 17.09 μm) which suggests that the thickness sustains for some time.

The white vertical lines in Fig. 1(d)-1(f) are artifacts caused by trigger mismatch of the laser source.

3.2 TPM results

We imaged the mouse ear with autofluorescence TPM before and 1 h after LPS treatment to observe microscopic changes during the inflammatory response. Visualization 1 and Visualization 2, respectively, are volume scan images of untreated and LPS treated mouse ear that show the several structures of the ear observable through TPM, such as the cells of the stratum corneum, epidermis, dermis layer structures, hair follicles, and blood vessels. Figure 2(a) and 2(c) were obtained from Visualization 1 and Fig. 2(b) and 2(d) were obtained from Visualization 2. In Fig. 2(a) and 2(b), blood vessels marked by red and blue arrows show changes in vessel diameter. Another vessel located at a different depth, which is marked by a yellow arrow, also shows a change in vessel diameter. Both vessels show approximately a 38% increase in diameter. In addition, we see that the image of 1 h post-treatment (Fig. 2(b) and 2(d), Visualization 2) is blurred compared to that of Fig. 2(a) and 2(c) (Visualization 1). We suspect that this is due to edema, which fills tissue with interstitial fluid. Also, since the overall thickness of the ear changes depending on the progression of inflammation, the precise imaging depth of each image was not reported. However, the appearance of the characteristic structures of some hair follicles and blood vessels allows us to determine that the images have been taken in the same location.

In order to direct immune cell migration towards inflammation-inducing challenge, we induced a wound by increasing the density of needle pricking around a single location of ear before applying LPS. To observe the migration of immune cells 1 h after LPS treatment, a time lapse image of a single image plane, with each frame given 20 sec interval, was taken for approximately 40 min duration (Fig. 3, Visualization 3, Visualization 4). In Fig. 3(a), epidermis cells, hair follicles, and blood vessels that contained flowing autofluorescent

#235702 Received 11 Mar 2015; revised 1 Jun 2015; accepted 9 Jun 2015; published 15 Jun 2015

fluorophores were clearly visible. However, we could not detect immune cell movement in the tissue (Visualization 3). In Fig. 3(b), immune cells appeared as granular structures. Each colored lines trace the path traveled by the target immune cells.

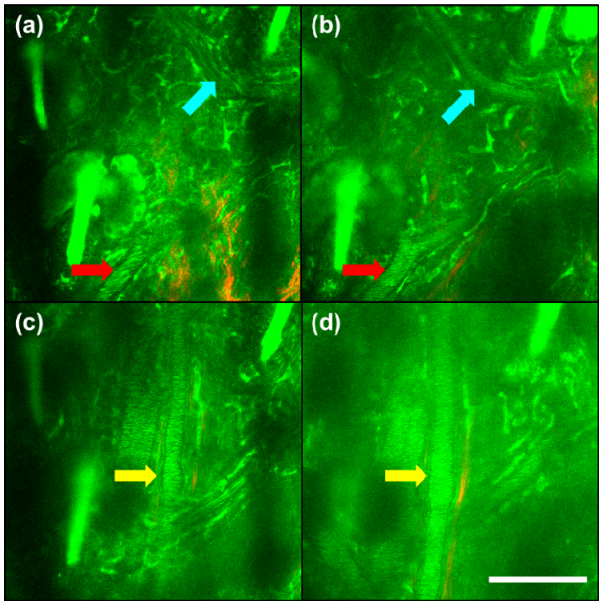

Fig. 2. TPM images of the mouse ear at two different fixed depth at different times show vasodilation as a result of inflammation. Approximately 38% capillary vasodilation occurred between 0 h (a, c) and 1 h (b, d) images. In both (b, d) the overall background noise has increased, which seems to be caused by increased light scattering due to tissue swelling from plasma leakage. Colored arrows indicate the location of blood vessels (Scale bar: 100 μm) (Visualization 1, Visualization 2).

The site of wound for inducing the inflammatory response is located at the bottom left corner of Fig. 3(b) but outside of imaging parameters. While the immune cells may not be reaching the wound site in the most direct way possible, and some immune cells even appear to be moving away from the wound site, the overall direction of migration of a significant majority of immune cells was towards the wound site (Visualization 4). In order to better visualize signal from mobile immune cells, we tracked a selected immune cell from Fig. 3(b) and displayed the time sequence images with enhanced contrast in Fig. 3(c). The arrow indicates the position of the selected immune cell.

3.3 Combined OCT and TPM system results

The same region of mouse ear was imaged by the combined OCT and TPM system, in order to visualize the immune response of mouse ear. The results are displayed in Fig. 4. The OCT in the combined system (Fig. 4(a)-4(f)) had a smaller FOV (1 x 1 mm) than that of the conventional OCT system. However, it still showed vascular distribution (Fig. 4(d)-4(f)) and the layered structure of the ear (Fig. 4(a)-4(c)) with similar clarity. Before inducing inflammation, normal thickness of mouse ear and low vascular density can be observed in Fig. 4(a) and Fig. 4(d), respectively.

In the combined system, the small TPM FOV is contained within the FOV of OCT, allowing comparison of observable microscopic and macroscopic changes in cell and tissue morphology of the target region. Before LPS treatment, a relatively dormant dermal microenvironment can be observed in the TPM image of Fig. 4(g) and Visualization 5.

LPS treatment resulted in visible changes in pinna thickness (Fig. 4(b), 4(c)) and vascular distribution (Fig. 4(e), 4(f)) compared to the untreated sample. The average ear thickness

#235702 Received 11 Mar 2015; revised 1 Jun 2015; accepted 9 Jun 2015; published 15 Jun 2015

before treatment was 276.36 μm ± 18.15 μm (Fig. 4(a)) and 398.72 μm ± 38.41 μm 1 h after treatment (Fig. 4(b)), yielding a 44.28% increase in thickness. 2 h after treatment (Fig. 4(c)), the thickness

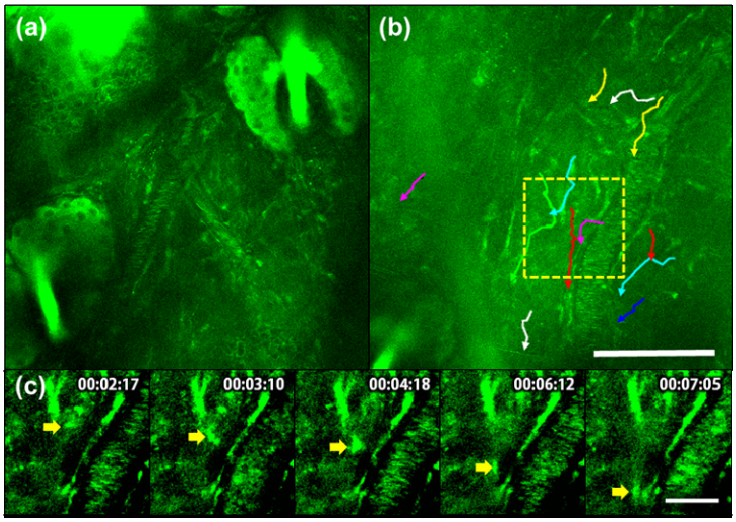

Fig. 3. Autofluorescence TPM (40 min time lapse) images of the inflammation response in untreated sample (a), (Visualization 3) and 1 h after LPS treatment (b), (Visualization 4) demonstrate immune cell migration post-treatment. Each line in (b) represents the path of immune cell migration. Time sequence images of the boxed region in (b) is shown in (c) with enhanced contrast. A selected immune cell is indicated by an arrow. From top to bottom the scale bar is 100 μm and 30 μm, respectively.

was 423.00 μm ± 30.80 was 423.00 μm. Furthermore, the mouse ear 1 hour after LPS treatment had an increase of volumetric capillary density compared to that of the untreated, as can be seen in Fig. 4(e). While correspondence of blood vessels may not be observed between Fig. 4(d)-4(f) and 4(g)-4(i), this is because the TPM images here were taken several micrometers above the plane where the main blood vessels visible in the angiographic images were located. Post-treatment images show immune cell infiltration as well (indicated by yellow arrowheads in Fig. 4(i), Visualization 6). Figure 4(j) shows a maximum intensity projection followed by time sequence images of immune cell movement of selected immune cells (indicated by blue and yellow arrows) from Fig. 4(i). However, unlike in the previous sample, cell migration was not yet observed 1 hour after LPS treatment, as can be seen in Fig. 4(h).

4. Discussion

In this present study we investigated the physiological and cellular level changes of LPS-induced skin inflammation through an imaging modality that provides complementary micro and macroscopic information within the same tissue model. Our results were consistent with previous reports on the dynamic characteristics of inflammation.

OCT resolved the entire cross section of the mouse ear at 10 micron resolution and provided morphological information of the layers of the ear in which we could distinguish the dermis and cartilage. Structural OCT images showed time dependent thickness change of the ear. Edema, which is a characteristic of tissue thickness change, was observed. In addition, the decrease of intensity signal may be due to the increase of interstitial fluid in the mouse ear which reduces the reflectivity of the tissue [29]. Enface angiographic OCT visualized changes in vascular distribution of the mouse ear by detecting the phase change of blood flow. Vasodilation was clearly observed as well as an increase in background signal, which may be

#235702 Received 11 Mar 2015; revised 1 Jun 2015; accepted 9 Jun 2015; published 15 Jun 2015

due to the increased blood flow into the capillaries in response to the inflammation [8, 30]. The background signal is due to our resolution limit, which was unable to resolve microvasculature.

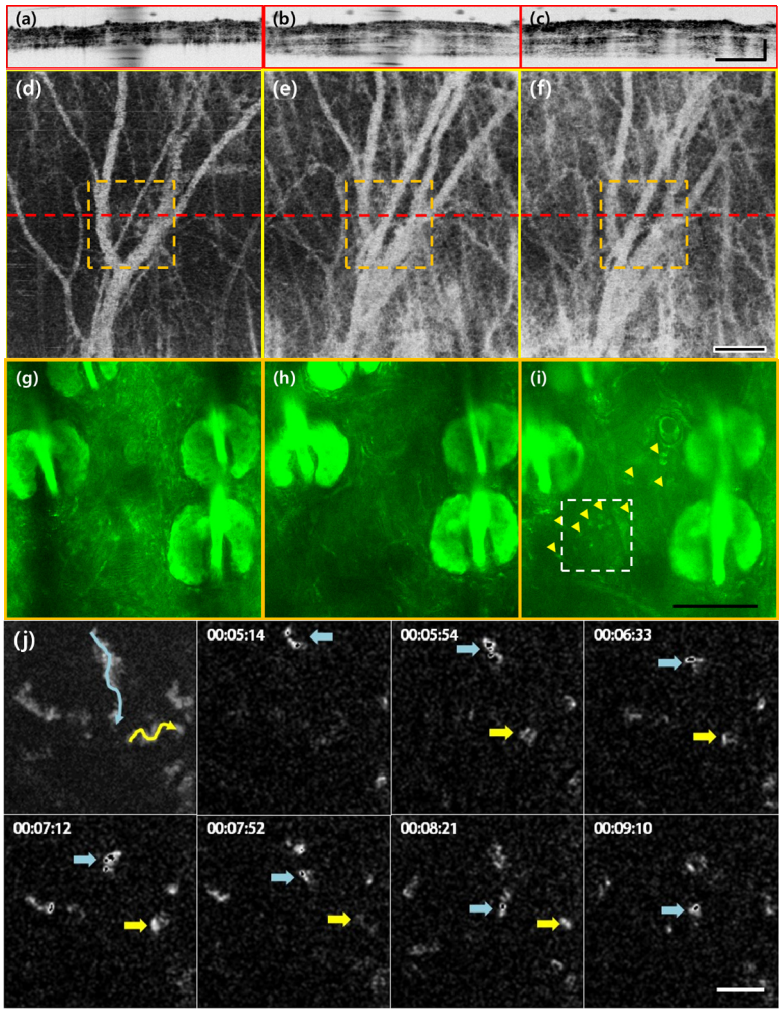

Fig. 4. (a-c), (d-f) and (g-i) are images of the same location taken by structural OCT, angiographic OCT, and TPM, which show the progression of vasodilation, tissue swelling, and immune cell migration, respectively. From left to right they are displayed by increasing time: untreated (a, d, g), 1 h (b, e, h) and 2 h after LPS treatment. Dashed red lines in enface angiographic OCT images (a-c) indicate the cross sectional location of the structural OCT image (d-f) and dashed orange squares indicate the FOV of TPM images (g-i, Visualization 5, Visualization 6). Yellow arrowheads in (i) point to the active immune cells. Figure 4(j) is a maximum intensity projection that displays the path taken by the immune cells in 4i followed by a time sequence of select neutrophil movement. The selected immune cells are marked by blue and yellow arrows. From top to bottom, the scale bars are 200, 200, 100, 50, and 20 μm, respectively.

In the TPM autofluorescence images, which visualized the stratum corneum, epidermis, dermis, hair follicles, and blood vessels, we were able to see capillary dilation and immune cell migration characteristic of inflammation, in real-time. Similar to the results of structural OCT, the TPM image post-treatment appears to be blurred. This is most likely because of the leakage of serum into the tissue due to the increase of blood vessel permeability. Interestingly, we also observed that the immune cells were migrating towards the direction of the wound.

#235702 Received 11 Mar 2015; revised 1 Jun 2015; accepted 9 Jun 2015; published 15 Jun 2015

Using two separate imaging platforms poses some limitations. Moving the sample from one imaging platform to the other is time consuming and may cause artifacts. Locating the same imaging area is difficult. In addition, to identify the TPM region of interest on the OCT projection is challenging. However, usage of a combined OCT and TPM system, which we have developed, overcomes these issues.

The combined OCT and TPM can simultaneously display in real-time the vascular distribution or cell dynamics previously and independently acquired by each system. Comparing the mouse ear 1 hour after treatment with the untreated mouse ear, changes in tissue thickness and vascular distribution was observed. Depending on the mouse, immune cell migration was observed 1 hour after treatment, as in the case of Fig. 3, and other times not until later, as observed in Fig. 4. We speculate that immune cell migrations may occur between 1 to 2 hours into the inflammation process, depending on the sensitivity of the individual mouse or spatial distribution of LPS treatment.

A limitation of autofluorescence imaging is that cell dynamics can only be observed through the movement of cells, since signal from both mobile and stationary cells are detected. Our characterization of immune cells was limited to the observation of movement of granular cells strong with NADH autofluorescence signals. In contrast to what was observed in normal tissue, bacterial challenge to induce an immune response invited a large population of small, mobile cells identified to be neutrophils or leukocytes into the inflamed tissues in previous reports, although they were labeled [18–20]. These cells were described to be "crawling" through connective tissue and had velocities ranging from 5 to 10 um/min [18], similar to our observations. Our granular structures were consistent with the description of a neutrophil which was reported to have relatively uniform NADH signals throughout its cytoplasm due to the fact that ATP synthesis of oxidative phosphorylation occurs in the cytosol as opposed to in the mitochondria [22].

Photobleaching and photodamage is another concern regarding autofluorescence imaging because higher laser power is necessary. Although we cannot formally dismiss the possibilities, we observed no appreciable signs of either even with our laser power and imaging time. We believe this is because the photons have sufficiently scattered within the 70 micrometers of our imaging depth.

Another limitation to this label-free optical method for studying the inflammation response is that it cannot track proteins crucial to the inflammatory response, making traditional methods of immunofluorescence, flow cytometry, etc. a necessity if one must study the subcellular characteristics of inflammation. In addition, dormant immune cells cannot be observed. Nonetheless, we have been able to observe in real time the various physiological and cellular characteristics of inflammation in living tissue using our optical technique, and believe that it will undoubtedly be useful for immune response studies.

In summary, we believe that combined OCT and TPM is appropriate for quickly assessing the inflammation response and we see a possibility for its application for studying the inflammation response induced by various skin diseases in preclinical and clinical studies.

Acknowledgments

This study was supported in part by the National R&D Program for Cancer Control (No. 1320220) by National Cancer Center Korea, the Engineering Research Center (2011-0030075), The Bio and Medical Technology Development Program (No. 2011-0019619, 2011-0019633) of the National Research Foundation (NRF) funded by the Korean government, a NRF grant (No. NRF-2014R1A2A1A12067510), and the Industrial Technology Innovation Program (No. 10048358) funded by the Ministry of Trade, Industry & Energy (MI, Korea). We would like to thank Benjamin Vakoc (Center for Biomedical OCT Research and Translation, Grant Number P41EB015903) for generously providing us with the MATLAB angiographic analysis code.